THE EFFECT OF FREEZE/THAW CYCLES ON THE PERFORMANCE AND MICROSTRUCTURE OF CEMENT-TREATED SOILS

Reza Jolous Jamshidi[1], Craig B. Lake[2], Peter Gunning[3] and Colin D. Hills[4]

[1] Ph.D., Civil and Resource Engineering Department, Dalhousie University, Canada.

[2] Professor, Civil and Resource Engineering Department, Dalhousie University, Canada.

[3] Associate Lecturer, Centre for Contaminated Land Remediation, University of Greenwich, United Kingdom.

[4] Professor, Centre for Contaminated Land Remediation, University of Greenwich, United Kingdom.

[*]Corresponding author. E-mail: craig.lake@dal.ca, Tel.: +1 (902) 494 3220

Abstract

In this paper, the performance and structural changes in cement-treated soils under influence of freeze/thaw (f/t) exposure are investigated. Specimens from plastic and compacted soil-cement mix designs were exposed to different f/t scenarios to study the influence of f/t dimensionality (i.e., one-dimensional vs three-dimensional exposure) and specimens' age at the time of f/t exposure on changes in their performance. Changes in hydraulic conductivity, unconfined compressive strength, and longitudinal resonant frequency of the specimens were studied under each exposure scenario. An examination of the microstructure of the f/t exposed and control specimens using transmitted light optical microscopy was also performed to evaluate how the soil-cement matrix was disrupted after exposure to f/t cycling. Observations showed increases in water content of the mix design (when wet of optimum water content), as well as increased specimen age at the time of exposure may increase f/t susceptibility. Contrary, comparison of the performance of the specimens exposed to one-dimensional and three-dimensional f/t exposure did not show any significant variation. Microstructural analysis of petrographic thin section samples from control and f/t exposed specimens showed that while optical microscopy can detect matrix disintegration for highly damaged specimens, it is not able to identify structural degradation at early stages of damage development.

INTRODUCTION

The treatment of soil with Portland cement is usually carried out to improve geotechnical performance in applications such as for use in the base layer for pavements, slope protection, and water retention systems. Treatment in this way allows a soil to meet performance specifications such as strength and hydraulic conductivity (ACI, 1990). Portland cement is also used in cement-based solidification/stabilization (S/S), a source-control remediation technique, where it is mixed with contaminated materials to mitigate the release of the contaminants to the surrounding environment (ITRC, 2011). As soils and contaminants are very heterogeneous and potential engineering application numerous, a wide variety of mix designs incorporating cement can be formulated.

Engineered cement-treated S/S systems are expected to maintain their structural integrity for decades (PASSiFy, 2010). However, it is suggested that under environmental exposure, similar factors that influence the long term performance of concrete (e.g. chemical attack, wet/dry (w/d) cycles, and freeze/thaw (f/t) exposure) may initiate these same degradation processes in S/S systems (Klich et al., 1999). During the design stage of cement-treated materials, w/d and f/t exposure tests have been routinely used to examine their durability (e.g., ASTM-D559 (1996) and ASTM-D560 (2003) (both withdrawn in 2012)). However, comparing the results of the laboratory investigations for cement-treated materials exposed to standard w/d and f/t cycles in the literature (e.g. Felt, 1955; Al-Tabbaa & Evans, 1998; Shihata & Baghdadi, 2001) suggest that f/t exposure may generally be a dominant factor controlling the durability of soil-cement materials.

The influence of f/t exposure upon the integrity and mechanical properties of compacted and plastic soil-cement has been widely studied in the literature (e.g. Felt, 1955; Dempsey & Thompson, 1973; Kettle, 1986; Pamukcu et al., 1994; Shihata & Baghdadi, 2001). Jamshidi and Lake (2015) and Jamshidi et al. (2015a) conducted extensive laboratory investigations focusing on changes in the hydraulic performance of cement-treated soils after f/t exposure. Increases of up to three orders of magnitude as well as minor decreases in the hydraulic conductivity values were observed after 12 cycles of f/t exposure. Both reductions and increases in UCS values were also reported in these studies. However, UCS changes did not correspond to the variations of hydraulic conductivity values obtained within each mix design. Jamshidi et al. (2015b) suggested that the impact resonance (IR) method may be a reliable non-destructive tool in predicting the potential trends in hydraulic conductivity changes of cement-treated soils subjected to cycles of f/t.

The majority of laboratory studies (e.g. ASTM-D560, 2003) evaluating f/t resistance subject the soil-cement to three-dimensional freezing, as opposed to a more realistic one-dimensional exposure scenario expected in the service environment. The influence of one-dimensional freezing on mechanical properties of soil-cement has been previously investigated (e.g. Dempsey & Thompson, 1973). However, possible correlation of the results between one- and three-dimensional exposure scenarios, do not appear to exist. Also, variations in the hydraulic performance of soil-cement under one-dimensional freezing conditions have not been addressed in the literature. In addition, a systematic examination of the micro/macro-structural changes in soil-cement materials undergoing freeze-thaw in this regard is lacking.

The current study examines the influence of f/t cycles on two mix designs employing cement to treat silty sand; representing compacted and plastic soil-cement conditions. Although it has been shown by Jamshidi et al. (2015a) and Jamshidi et al. (2015b) that damage may progress as the number of f/t cycles increases, a significant portion of the damage was shown to occur in the initial cycles of f/t. Given that the mechanism of the initiation of this damage is of interest, three cycles of f/t were performed for this study. Three-dimensional f/t exposure was performed upon immature samples (aged 16 days) and mature samples (aged over 110 days). Mature specimens from each mix design were also exposed to a one-dimensional freezing process. Hydraulic conductivity, unconfined compressive strength, and longitudinal resonant frequency (RF) measurements were performed on control and f/t exposed specimens for each of the exposure scenarios described above. Transmitted light microscopy was also conducted on petrographic thin sections obtained from specimens exposed to the various exposure and freezing scenarios, to examine potential mechanisms of degradation.

MATERIALS AND METHODS

Soil Materials Used For Soil-Cement Mixes

Selected size fractions from two soils (known as soil A and soil B) were blended to create the soil used in this study (i.e., referred to as soil SIII in table 1). Soil A consisted of a glacially-derived silty-sand (ASTM-D2487, 2011) and Soil B consisted of the fine-grained by-product of a quarry operation. Both soils were collected in Nova Scotia, Canada. An analysis performed on soil A and B indicate silica, aluminum, potassium, sodium, and iron as the major oxides present (Table 2). Quartz and feldspars were also identified as the main

66 crystalline phases in both soils based on an X-ray diffraction analysis shown in Figure 1.
67 Standard proctor tests (ASTM-D558, 2011) performed on the blended soils mixed with
68 10% by weight Portland-limestone blended cement (CSA type GUL) showed an optimum
69 water content (OWC) of approximately 11 percent and a maximum dry density of
70 approximately 1975 kg/m^3.

71 **Soil-Cement Specimen Preparation**

72 The two mix designs used in the study were chosen to represent compacted soil-cement
73 prepared at near OWC conditions (i.e. SIII(1.2) specimens (soil SIII stabilized at a
74 water/cement (w/c) ratio of 1.2) in Table 1), and plastic soil-cement prepared at slightly
75 over eight percent above OWC conditions (i.e. SIII(2.1) specimens (soil SIII stabilized at
76 a w/c ratio of 2.1) in Table 1). To prepare the specimens from each mix design, the soil,
77 cement and water were mixed using a drill-mounted paddle at the proportions presented in
78 Table 1. SIII(1.2) specimens were compacted in standard proctor molds in three layers in
79 accordance with ASTM-D558 (2011). SIII(2.1) specimens were placed into cylindrical
80 plastic molds (101 mm in diameter and 118 mm in height) in three layers, each layer being
81 tamped with 20 blows of a standard concrete slump testing rod to provide the required
82 consolidation. After placement, the molds were placed in sealed plastic bags for five days,
83 when specimens were extruded and kept in a 100% humidity moist room for further curing.

84 **F/T Conditioning of Specimens**

85 ***Immature- vs. Mature-Exposure***

86 Jamshidi and Lake (2015) showed that mature specimens exposed to 12 f/t cycles exhibit
87 higher amounts of damage compared to immature conditions. Non-destructive
88 examinations performed by Jamshidi et al. (2015a) and Jamshidi et al. (2015b) also showed
89 that a significant portion of the degradation during f/t exposure occurred in the initial f/t
90 cycles. Considering these observations, in the current study, immature and mature
91 specimens from each mix design (i.e., specimens cured for 16 days and over 110 days,
92 respectively) were exposed to three f/t cycles. The time period of 16 days was chosen based
93 on the work of Jamshidi et al (2015a) while the time period of 110 days was chosen to
94 reflect a curing time in which the majority of cement hydration would be complete,
95 minimizing further structural changes in soil-cement structure. Each f/t cycle consisted of
96 24 hours of three-dimensional freezing at -10±1°C followed by thawing in a 100%
97 humidity room at a temperature of 22±1°C. All specimens were saturated in a set-up
98 presented in method A of ASTM-D5084 (2010) under a minimum back-pressure of 524
99 kPa and a confining pressure of over 558 kPa for a duration of at least seven days before
100 f/t exposure. Previous work by Goreham et al. (2012) showed how for similar cement
101 contents, β -value measurements were greater than 95% for the saturation conditions
102 employed in this work.

103 ***One- vs. Three-Dimensional Specimen Freezing***

104 Ground freezing occurs due to boundary conditions created by sub-zero air temperatures.
105 Heat flux occurs one-dimensionally, resulting in progressive downward freezing of the soil.
106 In the current study, mature specimens from both mix (i.e., SIII(1.2) and SIII(2.1)) designs
107 were exposed to three cycles of one-dimensional freezing followed by thawing in the 100%

humidity room. The changes in the performance of these specimens were then compared to similar specimens exposed to three-dimensional f/t.

A test set-up shown in Figure 2 was used to one-dimensionally freeze duplicate specimens from each mix design. Specimens were placed in a plexiglass tube with a wall thickness of 1.5 cm covered with approximately 1.2 cm of fibreglass insulation. One-dimensional flow of temperature during the freezing process was confirmed by Mcknight-Whitford (2013) in a similar test setup. To provide intimate contact between specimens and the plexiglass tube walls (i.e. the interior surface of plexiglass tubes), layers of plastic wrap were placed around each specimen and the final surface was coated with vacuum grease prior to the placement in the tubes. A dummy sample, having a similar mix design to specimens being tested, with a height of approximately 5 cm was placed underneath each specimen to facilitate achieving sub-zero temperatures at the bottom of the specimens during the freezing process. A mixture of ice and water was used to maintain the temperature at the base of the dummy sample at 0^{o}C. A compact refrigerated circulator (i.e. HAAKE DC30 liquid chiller with a K10 bath) was used to circulate a mix of water and antifreeze at a temperature of -10±1^{o}C through the stainless steel caps placed on top of each of the duplicate specimens. The whole set-up was placed in a room with an ambient temperature of 3±1^{o}C to provide the required working conditions for the compact refrigerated circulator. Thermocouples were placed between the specimens and the dummy samples to monitor the temperature changes at the base of the specimens and to ensure complete freezing of the specimens in order to provide proper comparison to the three-dimensional freezing conditions. Each freezing phase lasted for three days, after which specimens were

extruded and placed in a moist room for approximately 24 hours for complete thawing. This process was repeated for a total of three f/t cycles.

Specimen Testing

Hydraulic conductivity, unconfined compressive strength (UCS), and longitudinal resonance frequency (RF) measurements were performed on the control and exposed specimens to monitor the changes in the performance of each mix design under different exposure scenarios and freezing conditions. Transmitted light microscopy was also performed on petrographic thin sections obtained from control and f/t exposed specimens in order to provide information regarding the microstructural changes and damage propagation mechanisms under various exposure conditions. A summary of the testing procedures used in the study follows.

Hydraulic Conductivity

Duplicate specimens were tested for hydraulic conductivity values before (i.e. control) and after three cycles of f/t exposure. General guidelines suggested in method A of ASTM-D5084 (2010) (i.e. constant head flexible-wall method) were followed during each test. Test duration ranged from 3 days to 2 weeks depending on the hydraulic conductivity of the specimens. Permeation was performed under a hydraulic gradient ranging from 29 to 60. The test was continued until a steady hydraulic conductivity value was achieved as described in the standard.

Impact Resonance (IR)

Vibration-based non-destructive techniques have been used for structural health monitoring purposes in various applications (e.g. Nagy, 1997; Sansalone, 1997; Shah et al., 2000; Jin & Li, 2001; Gheorghiu et al., 2005). Since resonant frequency (RF) of a material measured using these techniques is related to its physical properties including density, shape, and the dynamic modulus of elasticity (Malhotra, 2011), it can be used as a reliable indicator for monitoring the changes in the material due to external stresses. Jamshidi et al. (2015b) showed that the IR method, as an example of vibration-based non-destructive techniques, can be used for early detection of damage in cement-treated soils during exposure to cycles of f/t.

In the current study, longitudinal resonance frequency (RF) of specimens was measured using the IR method, before f/t exposure and subsequently at the end of the thawing phases of cycles 1, 2, and 3. The tests followed the general procedures presented in ASTM-C215 (2008). Impact load was generated using a steel ball with a diameter of 9.5 mm attached to a plastic band. An accelerometer (PCB model 352C68) and a Freedom Data PC Platform (Olson Instruments Inc.) were used for the data acquisition and signal processing. A bandwidth filter of 500-15000 Hz, sampling rate of 500 KHz, and record size of 8192 samples were used during the test. Each test consisted of five trials on the specimen with the average values being reported as the RF.

Unconfined Compressive Strength (UCS)

Unconfined compressive strength (UCS) measurements were performed on duplicate specimens for the control and f/t exposed conditions. Sulfur-capped specimens were subjected to a vertical deformation rate of 0.5 mm/min during the loading process.

Transmitted Light Optical Microscopy

A study of the microstructural changes in the exposed specimens using petrographic methods can provide an insight on the mechanisms of damage formation during f/t exposure. Petrographic thin section samples were prepared by a specialized laboratory at the Geology and Earth Sciences Department of Dalhousie University. Thin sections were taken from horizontal and vertical planes of resin impregnated samples from the control and exposed specimens. An examination of the thin sections was performed using a Nikon Optiphot-Pol polarized light microscope equipped with a 12 megapixel digital scanning camera (Kontron ProgRes 3012).

RESULTS AND DISCUSSION

A summary of the hydraulic conductivity, UCS, and resonant frequency results obtained from the study is presented in Table 3. Below is a discussion of these results as well as microstructural changes observed from the thin section samples using transmitted light microscopy.

Hydraulic Conductivity

Figure 3 shows the influence of water content in the mix design on hydraulic conductivity of the treated soil under both immature and mature curing conditions (i.e. without f/t exposure). Results from measurements presented in Jamshidi and Lake (2015) on a similar soil at different water contents are also presented in Figure 3 to better demonstrate the variations with respect to OWC conditions. The results show that the lowest hydraulic conductivity can be achieved by preparing mix designs slightly wetter than OWC conditions. Hammad (2013) previously showed that for specimens cured for 28 days, the lowest hydraulic conductivity occurred at a water content ranging from 2 to 6 percent above the standard proctor OWC conditions for a similar soil. It is hypothesized that this water content range produced the lowest hydraulic conductivity because, similar to compacted clay soils (Mitchell et al., 1965; Benson and Daniel, 1990), the samples slightly wet of optimum produced a more dispersed structure and a resulting soil kneading action during compaction at this moisture level (i.e. near its plastic limit). The resulting fabric is more aligned in a direction perpendicular to flow and any clods are kneaded during the compaction process. Figure 3 shows that hydraulic conductivity values increase at a slow "rate" as water content is increased from near OWC (11%) up to a moisture content of 18%, after which the hydraulic conductivity seems to be very sensitive to a one percent increase in moisture content (i.e. 19%). This is possibly due to the excessive bleeding of the water during preparation of mixtures at high water contents creating high porosity areas within the final structure.

212 Hydraulic conductivity values also seem to be sensitive to water content changes when
213 below OWC conditions. Approximately a three to four orders of magnitude increase in
214 hydraulic conductivity is observed as the water content during compaction of the mix
215 design is decreased from a value of 11% (i.e., near OWC conditions) to 9% (slightly below
216 OWC conditions). This increase is likely due to a combination of less water available for
217 hydration and/or insufficient "lubrication" of soil and cement particles during the
218 compaction process to assist with the "kneading" action (Mitchell et al., 1965; Benson and
219 Daniel, 1990). Figure 3 also shows a decrease of as much as two orders of magnitudes in
220 the hydraulic conductivity values between immature and mature measurements as a result
221 of the progression of the hydration process in the specimens.

222 Changes in the hydraulic conductivity values for SIII(1.2) and SIII(2.1) specimens obtained
223 under various f/t exposure conditions are presented in Figure 4. After three cycles of three-
224 dimensional f/t exposure, a wide range of changes in hydraulic conductivity values was
225 observed which appears to be dependent on the curing conditions and mix design. For the
226 SIII(1.2) mix design, immature specimens showed a slight reduction in hydraulic
227 conductivity values, while mature specimens exhibited an increase of about one order of
228 magnitude. Also of note is that the hydraulic conductivity values after f/t exposure, even
229 though they have undergone an increase, remain low (less than 10^{-10} m/s). Under similar
230 conditions, immature and mature specimens from SIII(2.1) showed increases of about 12
231 and 320 fold in the hydraulic conductivity values, respectively. Increase in hydraulic
232 conductivity values after f/t exposure is likely a result of crack initiation and subsequent
233 structural degradation due to expansion of pore water in soil-cement during the freezing
234 process.

The theory of damage development in cement-based materials during f/t exposure is discussed in previous research studies (e.g. Powers, 1945; Setzer, 2001). Conversely, the decrease in hydraulic conductivity values after f/t exposure of immature SIII(1.2) is likely due to the interaction of the continuing hydration of cement, as well as various healing mechanisms (e.g. mineral precipitation) acting in parallel with the deleterious effect of the f/t process. Hydraulic conductivity recovery of damaged soil-cement specimens after post-exposure curing was also reported in Jamshidi and Lake (2015).

Examination of one-dimensional freezing conditions compared to three-dimensional freezing conditions has been conducted in the literature by Othman & Benson (1993) for compacted clay soils. Othman & Benson (1993) showed that f/t dimensionality has negligible influence on the changes in the hydraulic performance and on the crack formation pattern in compacted clay specimens. Comparing the hydraulic conductivity changes in mature specimens exposed to one- and three-dimensional freezing conditions in the current study (Figure 4) also shows changes in the hydraulic conductivity values are within the same order of magnitude for both freezing scenarios.

Longitudinal Resonant Frequency (RF)

Figure 5 presents the RF values measured on specimens at control conditions (i.e. cycle 0) and subsequently after 1st, 2nd, and 3rd f/t cycles. Values obtained for control specimens show mature specimens exhibit higher RF values compared to immature specimens, which is a result of increased structural integrity due to longer curing. Also, both immature and mature SIII(1.2) specimens show higher RF values compared to SIII(2.1) specimens. Higher RF values suggest a higher stiffness of these specimens. Values are also in

agreement with lower hydraulic conductivity measurements presented in the previous section.

For SIII(1.2)-immature specimens, RF values were relatively constant (slightly over 12000 Hz) through different f/t cycles, which suggests minor structural changes. This was in agreement with the slight reductions in hydraulic conductivity values of these specimens after f/t exposure. For SIII(1.2) mature specimens exposed to three-dimensional f/t, RF values showed over 1000 Hz reduction after the initial cycle and reached a value of about 10800 Hz (i.e. a total decrease of approximately 2600 Hz) at the end of the third cycle. Reductions in the RF values were in agreement with the increases observed in the hydraulic conductivities of these specimens (see Figure 4). For SIII(1.2) mature specimens exposed to one-dimensional freezing conditions, RF values showed only minor variations over three f/t cycles, which is in contrast to approximately five times increase observed in their hydraulic conductivity values. However, as noted previously, the final hydraulic conductivity values are still lower than 10^{-10} m/s, suggesting that the specimens are still relatively intact.

For SIII(2.1)-immature and SIII(2.1)-mature specimens, average RF values dropped from 8300-9600 Hz to values close to 2000 Hz after three cycles of f/t. This extensive drop in RF values is consistent with several orders of magnitude change in hydraulic conductivity for this mix, both observations suggesting a significant change in structure within the soil-cement specimens.

For the mature specimens tested from SIII(2.1) mix design, variations of results for one- and three-dimensional freezing conditions were insignificant. Also, irrespective of

exposure scenario, the initial cycle had a significant effect in the degradation of the specimens, resulting in over 38 percent reduction in the RF values.

Unconfined Compressive Strength (UCS)

Trends in the UCS values for the treated soil at w/c ratios ranging from 1 (below OWC) to 2.1 is shown in Figure 3. Data presented in Figure 3 include both measurements performed in this study and UCS measurements presented in Jamshidi and Lake (2015) on a similar soil treated at different w/c ratios. Maximum UCS values appear to correspond with the OWC, with values decreasing at a higher rate above OWC. Observations by Felt (1955) previously showed that for non-plastic soils the maximum UCS occurs slightly below the OWC obtained from the standard proctor test.

Figure 6 presents the results of UCS testing for SIII(1.2) and SIII(2.1) specimens after three cycles of f/t exposure. On average, SIII(1.2) specimens showed a general increasing trend (with a maximum increase of about six percent) in UCS values for both immature and mature exposure conditions. SIII(2.1)-immature showed an average reduction of 17 percent after f/t exposure while SIII(2.1)-mature remained relatively unchanged after three-dimensional f/t exposure. A 19 percent reduction was observed for similar specimens exposed to one-dimensional freezing. Comparing the UCS measurements to the observations on hydraulic conductivity changes for similar mix designs, it is apparent that UCS is not a suitable indicator of the changes in the hydraulic performance of cement-treated soils. For instance, it is possible that micro-crack formations during the freezing process can lead to increases in the hydraulic conductivity values, while under similar conditions the compressive forces applied during the UCS test can cause the micro-cracks

301 to contribute to the strength of the specimen as a result of friction development on the crack
302 walls.

303 **Optical Microscopy**

304 An examination of the microstructure of the cement-treated soil using transmitted light
305 optical microscopy was performed to examine how the soil-cement matrix was disrupted
306 after exposure to f/t cycling. Comparison of the micrographs between the horizontal and
307 vertical planes obtained from control and f/t exposed specimens did not suggest any
308 noticeable spatial variation in the soil-cement structure and the damage formation
309 mechanisms. Typical micrographs obtained from specimens under control and three-
310 dimensional f/t exposed conditions are presented in Figure 7. The blue color in the
311 micrographs presented in Figure 7 represents the pore structures that were filled with the
312 resin used during the impregnation of the samples prior to thin section preparation.

313 The soils used in the study appear to be "young", in the respect that they contain minerals
314 associated with the disintegration/degradation of igneous and metamorphic rocks. These
315 minerals (which are relatively thermodynamically unstable), form angular, coarser clasts.
316 Minerals identified in the coarser fraction include microcline, plagioclase, ferromagnesian
317 minerals, and micas. Some of the clasts present in the soil exhibit signs of degradation,
318 including micro-cracking, suggesting that prior to use in the study, they were subject to
319 mechanical or environmental loading (see images A, B, and G in Figure 7).

320 Discrete incidents of high porosity areas were observed in control samples from both
321 SIII(1.2) and SIII(2.1) mix designs (see patches of blue color in images C and G in Figure

7). These features were likely induced during the placement of the specimens as a result of poor compaction and/or localized high water content areas in the matrix. It should be noted that the images presented in Figure 7 are in scales of millimeters and hence there were hundreds of potential images. Those presented in Figure 7 are considered typical based upon visual observations of the entire thin sections.

Considering the control conditions in Figure 7, the microstructure in samples from SIII(2.1) with higher w/c ratio, appears less dense (see images A and C in Figure 7), especially at the matrix/aggregate interface. SIII(1.2) samples prepared at lower w/c ratio have a denser packing and a less intense blue color (see images E and G in Figure 7).

Under the exposed conditions, in the thin sections from SIII(2.1)-immature specimens ($K_{exposed}/K_0 \approx 12$), minor matrix disruptions in scattered areas throughout the paste were noticeable as is shown in micrographs presented in Figure 8. For the same mix design under mature three-dimensional f/t exposure (i.e. SIII(2.1)-mature with a $K_{exposed}/K_0 \approx 320$), more evidence of matrix disruption as well as some micro-cracking along the paste-aggregate interface were observed (Figure 8). Damage in the thin sections from SIII(2.1)-mature was also evident by comparing the thin sections even at a larger scale as is shown in Figure 9 (note the increased intensity of blue color in exposed sample as compared to the control sample). It can also be seen in Figure 9 that damage formation in soil-cement, at least at the high cement content used in this study, doesn't follow the mechanisms suggested for compacted clay (i.e. parallel ice lens formation), which is likely a result of higher tensile strength of these materials due to the binding capacity of cement hydration products.

343 Considering SIII(1.2)-immature samples, the damage was less evident, although some
344 disruption of the matrix was observed (Figure 10). This was despite the reduction of the
345 hydraulic conductivity values in this mix design after f/t exposure. This reduction is likely
346 a result of the decreased hydraulic conductivity of the paste due to the hydration process
347 and the isolation of the disrupted areas by unaffected materials. In SIII(1.2)-mature,
348 although approximately ten times increase in the hydraulic conductivity values were
349 observed after three-dimensional f/t exposure, only minor scattered degradation of the
350 matrix were observed during the analysis (Figure 10). It should be again noted that although
351 increases in hydraulic conductivity were observed, the final hydraulic conductivity value
352 of the SIII(1.2) mixtures was less than 10^{-10} m/s and hence tend to agree with the
353 microscope observations. Similar to the SIII(2.1) mature mix samples, no ice lens
354 formation was observed.

355 Microstructural analysis of one-dimensionally exposed specimens did not reveal any
356 obvious differences in the mechanisms of f/t damage compared to three-dimensional
357 exposure. More damage (in terms of matrix-aggregate interface cracking and matrix
358 disruption) was observed in the micrographs obtained from SIII(2.1) specimens (i.e. one-
359 dimensional f/t), with higher hydraulic conductivity changes. This was compared to minor
360 structural changes in the SIII(1.2) specimens with slight increases in the hydraulic
361 conductivity values (Figure 11).

362 Results of the microstructural analysis performed show that there are obvious limitations
363 on sample observation using transmitted light microscopy. The degree of microstructural
364 disturbance between samples and within individual samples is not as obvious as

anticipated, even though other test methods showed a reduction in structural integrity for most of the scenarios investigated. Thus, the use of transmitted light microscopy may not be able to resolve the early stages of (sub-microscopic) matrix disruption, whereas the other indirect analytical methods (i.e, hydraulic conductivity, UCS, and RF measurements) employed have this capability. However, it was established that microstructural damage was mainly in the form of matrix disruption; cracking within the matrix, and cracking at aggregate boundaries.

CONCLUSIONS

Cement-treated silty sand specimens prepared at two w/c ratios representing compacted and plastic soil-cement mix designs were exposed to three cycles of freeze/thaw (f/t). Various sample ages (i.e. immature vs. mature) and f/t dimensionality (i.e. one-dimensional vs. three-dimensional) scenarios were investigated. Changes in performance of the specimens were monitored using hydraulic conductivity, UCS, and longitudinal RF measurements. Also, microstructural degradation of the specimens were evaluated by studying petrographic thin section samples obtained from the specimens, using transmitted light optical microscopy technique. The following conclusions can be drawn from the results.

1. Performance measurements on soil-cement specimens prepared over a wide range of water contents (i.e. without f/t exposure) showed that minimum hydraulic conductivity likely occurs at water contents slightly above optimum water content. In this study, hydraulic conductivity values increased at a slow "rate" as water content is increased from near OWC (11%) up to a moisture

content of 18%, after which the hydraulic conductivity seemed to be very sensitive (i.e. hydraulic conductivity increased) to a one percent increase in moisture content (i.e. 19%). The maximum UCS possibly occurs at water contents near or slightly below optimum water contents. Hydraulic conductivity values seem to be more sensitive (i.e. hydraulic conductivity increased) to changes in the water contents towards dryer mix designs. Approximately a three to four orders of magnitude increase in hydraulic conductivity is observed as the water content during compaction of the mix design is decreased from a value of 11% (i.e. near OWC conditions) to 9% (slightly below OWC conditions). UCS values are more sensitive (i.e. decrease in UCS values) to changes in the water contents towards wetter mix designs, with respect to optimum water content conditions.

2. Specimens exposed to three f/t cycles exhibited a wide range of performance changes including minor enhancement of the performance (possibly due to the interaction of f/t degradation mechanisms with the hydration/healing processes) as well as increases in the hydraulic conductivity values and decreases in the UCS and RF values (i.e. performance degradation). Specimens prepared at higher water content (i.e. SIII(2.1)) exhibited more damage after f/t exposure compared to the dryer mix design (i.e. SIII(1.2)). Also, it was found that mature specimens are more susceptible to f/t exposure compared to immature specimens; an observation discussed in detail in Jamshidi and Lake (2015).
3. Under the testing conditions applied in the study, no significant variation in the performance of the specimens exposed to one-dimensional and three-

dimensional f/t exposure was observed. This may suggest while one-dimensional f/t studies better mimic the exposure mechanisms expected in the field, laboratory investigation of soil-cement using three-dimensional f/t exposure scenarios can still provide a reliable estimation of the performance degradation.

4. Microstructural analysis of petrographic thin section samples from control and f/t exposed specimens showed that optical microscopy is not able to identify structural degradation at early stages of damage development, suggesting presence of possible sub-microstructural disruption mechanisms. For highly damaged specimens (i.e. in terms of hydraulic conductivity changes), however, signs of matrix disintegration as well as matrix-aggregate interface cracking were identified.

REFERENCES

ACI (American Concrete Institute). (1990). "Report on soil cement." *ACI230.1R-90* Farmington Hills, MI.

Al-Tabbaa, A. and Evans, C.W. (1998). "Pilot in situ auger mixing treatment of a contaminated site. part 1: treatability study." *Proceedings of the Institution of Civil Engineers: Geotechnical Engineering*, **131**(1):pp.52–59. doi:10.1680/igeng.1998.30005.

ASTM-C215 (ASTM International). (2008). "Standard test method for fundamental transverse, longitudinal, and torsional resonant frequencies of concrete specimens." West Conshohocken, PA: doi:10.1520/c0215-08.2.

ASTM-D2487 (ASTM International). (2011). "Standard practice for classification of soils for engineering purposes (unified soil classification system)". West Conshohocken, PA: doi:10.1520/d2487-11.

ASTM-D5084 (ASTM International). (2010). "Standard test methods for measurement of hydraulic conductivity of saturated porous materials using a flexible wall permeameter." West Conshohocken, PA: doi:10.1520/d5084-10.

ASTM-D558 (ASTM International). (2011). "Standard test methods for moisture-density (unit weight) relations of soil-cement." West Conshohocken, PA: doi:10.1520/d0558-11.

ASTM-D559 (ASTM International). (1996). "Standard test methods for wetting and drying compacted soil-cement mixtures." West Conshohocken, PA.

ASTM-D560 (ASTM International). (2003). "Standard test methods for freezing and thawing compacted soil-cement mixtures." West Conshohocken, PA: ASTM International. doi:10.1520/d0560-03.

Benson, C.H. and Daniel, D. E. (1990). "Influence of clods on hydraulic conductivity of compacted clay." Journal of Geotechnical Engineering (ASCE) 116(12):1811-1830.

Dempsey, B.J. and Thompson, M.R. (1973). "Vacuum saturation method for predicting freeze-thaw durability of stabilized materials." *Highway Research Record 442*. Highway Research Board, US National Research Council, pp. 44–57.

Felt, E.J. (1955). "Factors influencing physical properties of soil-cement mixtures." *Highway Research Board Bulletin*, 108:pp.138–162.

Gheorghiu, C., Rhazi, J.E. and Labossière, P. (2005). "Impact resonance method for fatigue damage detection in reinforced concrete beams with carbon fibre reinforced polymer." *Canadian Journal of Civil Engineering*, 32(6):pp.1093–1102. doi:10.1139/l05-064.

Goreham, V., Lake, C.B., and Yuet, P.K. (2012). "Characterizing porosity and diffusive properties of monolithic cement-based solidified/stabilized materials." ASTM Geotechnical Testing Journal, 35(4):529-538.

Hammad, A. (2013). "Evaluation of soil-cement properties with electrical resistivity." *M.A.Sc. Thesis*, Civil and Resource Engineering Department, Dalhousie Univesity, Halifax, NS.

ITRC (2011). "Development of performance specifications for solidification/stabilization (technical/regulatory guidance)." The Interstate Technology & Regulatory Council, Solidification/Stabilization Team. Washington, DC.

Jamshidi, R. and Lake, C.B. (2015). "Hydraulic and strength performance of three cement-stabilized soils subjected to cycles of freezing and thawing." *Canadian Geotechnical Journal*, 52(3): 283-294, 10.1139/cgj-2014-0100.

Jamshidi, R., Lake, C.B., and Barnes, C. (2015a). "Examining freeze/thaw cycling and its impact on the hydraulic performance for a cement-treated silty sand." *ASCE Journal of Cold Regions Engineering*, 10.1061/(ASCE)CR.1943-5495.0000081, 04014014.

Jamshidi, R., Lake, C.B., and Barnes, C. (2015b). "Evaluating impact resonance testing as a tool for predicting hydraulic conductivity and strength changes in cement-stabilized soils." *ASCE Journal of Materials in Civil Engineering*, 10.1061/(ASCE)MT.1943-5533.0001318, 04015051.

Jin, X. and Li, Z. (2001). "Dynamic property determination for early-age concrete." *ACI Materials Journal*, 98(5):pp.365–370.

Kettle, R.J. (1986). "The assessment of freeze-thaw damage in cement stabilized soils". *Proceedings of Research on Transportation Facilities in Cold Regions (ASCE).* Edited by O. B. Andersland & F. H. Sayles. pp. 16–31.

Klich, I., Batchelor, B., Wilding, L.P. and Drees, L.R. (1999). "Mineralogical alterations that affect the durability and metals containment of aged solidified and stabilized wastes." *Cement and Concrete Research*, 29:pp.1433–1440.

Malhotra, V.M. (2011). "Nondestructive tests." *Significance of Tests and Properties of Concrete and Concrete-Making Materials (STP 169D)*. Edited by J. F. Lamond & J. H. Pielert. West Conshohocken, PA: ASTM International, pp. 314–334.

Mcknight-Whitford, H. (2013). "Development of an experimental device for monitoring frost heave in soils." M.A.Sc. Thesis, Civil and Resource Engineering Department, Dalhousie Univesity, Halifax, NS.

Mitchell, J. K., Hooper, D. R. and Campanella, R. G. (1965). "Permeability of compacted clay." Journal of Soil Mechanics and Foundations Division (ASCE) 91(SM4): 41-65.

Nagy, A. (1997). "Determination of E-modulus of young concrete with nondestructive method." *ASCE Journal of Materials in Civil Engineering*, 9(1):pp.15–20. doi:10.1061/(asce)0899-1561(1997)9:1(15).

Othman, M.A. and Benson, C.H. (1993). "Effect of freeze-thaw on the hydraulic conductivity and morphology of compacted clay." *Canadian Geotechnical Journal*, 30:pp.236–246.

Pamukcu, S., Topcu, I.B. and Guven, C. (1994). "Hydraulic conductivity of solidified residue mixtures used as a hydraulic barrier." *Hydraulic Conductivity and Waste Contaminant Transport in Soil (STP 1142)*. Edited by D. E. Daniel & S. J. Trautwein. Philadelphia, PA: ASTM International, pp. 505–520. doi:10.1520/stp23905s.

PASSiFy (2010). "Performance assessment of solidified/stabilised waste-forms, an examination of the long-term stability of cement-treated soil and waste." A Joint Research Consortium, Final Report. CL:AIRE Project RP16. <http://www.claire.co.uk> (October 29, 2015).

507 Powers, T.C. (1945). "A working hypothesis for further studies of frost resistance of
508 concrete." *Bulletin no. 5,* Portland Cement Association. Research and Development
509 Laboratories., 41:pp.245–272.

510 Sansalone, M. (1997). "Impact-Echo: the complete story." *ACI Structural Journal*,
511 94(6):pp.777–786.

512 Setzer, M.J. (2001). "Micro-ice-lens formation in porous solid." *Journal of Colloid and*
513 *Interface Science."* 243(1):pp.193–201. doi:10.1006/jcis.2001.7828.

514 Shah, S.P., Popovics, J.S., Subramaniam, K. V. and Aldea, C. (2000). "New directions in
515 concrete health monitoring technology." *ASCE Journal of Engineering Mechanics*,
516 126(7):pp.754–760.

517 Shihata, S.A. and Baghdadi, Z.A. (2001). "Long-term strength and durability of soil
518 cement." *ASCE Journal of Materials in Civil Engineering*, 13(3):pp.161–165.

519

Table 1: Summary of the mix designs utilized for SIII(1.2) and SIII(2.1).

Mix designation	W/c ratio	Cement content, percent (dry weight of soil)	Mixing method*	Composition of the soil used (i.e. soil SIII) by dry weight, percent					ASTM classification of the blended soil
				Soil A				Soil B <0.08 mm	
				9.50-4.75 mm	4.75-1.20 mm	1.20-0.30 mm	0.30-0.08 mm		
SIII(1.2)	1.2	10	C	9	30	21	10	30	Silty sand
SIII(2.1)	2.1	10	S						

*C: compaction, S: self-consolidation.

Table 2. Mineralogical composition of soil A and soil B.

	SiO_2	Al_2O_3	K_2O	Na_2O	Fe_2O_3	LOI (1000°C)*	Other
Soil A	71.82	14.57	3.27	3.03	2.66	2.41	2.24
Soil B	65.65	15.31	4.02	3.08	5.66	1.17	5.11

*LOI: Loss on ignition

Table 3: Summary of performance test results under control and exposed conditions.

Test		Hydraulic conductivity, m/s (Relative standard deviation, %)				UCS, MPa (Relative standard deviation, %)				Longitudinal resonance frequency, kHz (Relative standard deviation, %)							
		3D		1D		3D		1D		3D				1D			
Exposure condition		Control	Exposed	Control	Exposed	Control	Exposed	Control	Exposed	Control	Cycle 1	Cycle 2	Cycle 3	Control	Cycle 1	Cycle 2	Cycle 3
SIII(1.2)	Immature	3.8×10^{-11} (38.7)	3.5×10^{-11} (36.2)	-	-	10.6 (4.0)	10.8 (0.5)	-	-	12.4 (1.5)	12.3 (1.2)	12.2 (1.2)	12.4 (2.1)	-	-	-	-
	Mature	5.9×10^{-12} (10.2)	5.7×10^{-11} (68.4)	2.0×10^{-12} (18.0)	1.1×10^{-11} (5.3)	11.2 (0.7)	11.7 (7.6)	-	11.9 (9.1)	13.4 (1.4)	12.0 (4.9)	12.2 (4.8)	10.8 (6.3)	12.8 (0.5)	12.6 (1.0)	12.7 (0.4)	12.6 (0.6)
SIII(2.1)	Immature	3.4×10^{-9} (11.8)	4.0×10^{-8} (19.0)	-	-	3.0 (3.3)	2.5 (4.0)	-	-	8.4 (2.2)	4.8 (7.6)	3.3 (1.9)	2.5 (2.4)	-	-	-	-
	Mature	2.1×10^{-10} (2.4)	6.8×10^{-8} (48.2)	2.9×10^{-10} (1.8)	2.4×10^{-7} (60.3)	3.7 (10.5)	3.6 (6.7)	-	3.0 (22.6)	9.6 (1.6)	4.6 (3.3)	3.0 (1.0)	2.0 (1.5)	9.9 (0.3)	6.1 (1.0)	3.6 (11.1)	2.6 (52.3)

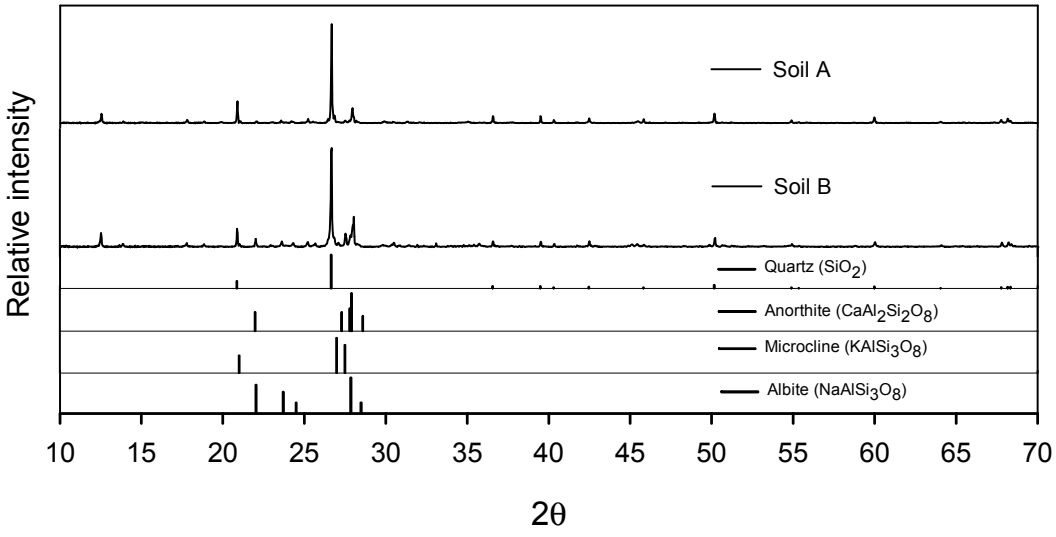

Figure 1: X-ray diffraction test results performed on powder samples from Soil A and B.

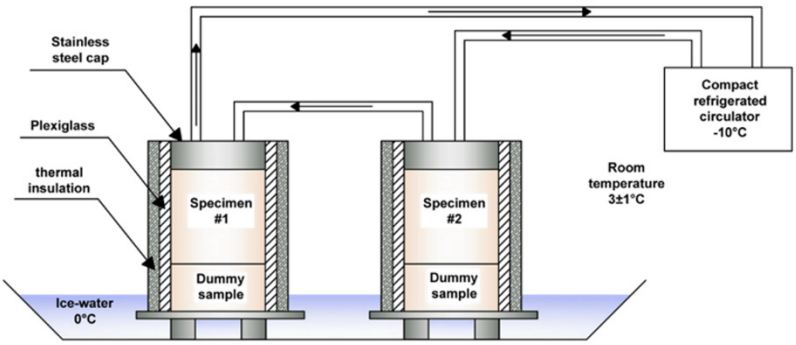

Figure 2: The set-up utilized for one-dimensional freezing of the cement-treated soils.

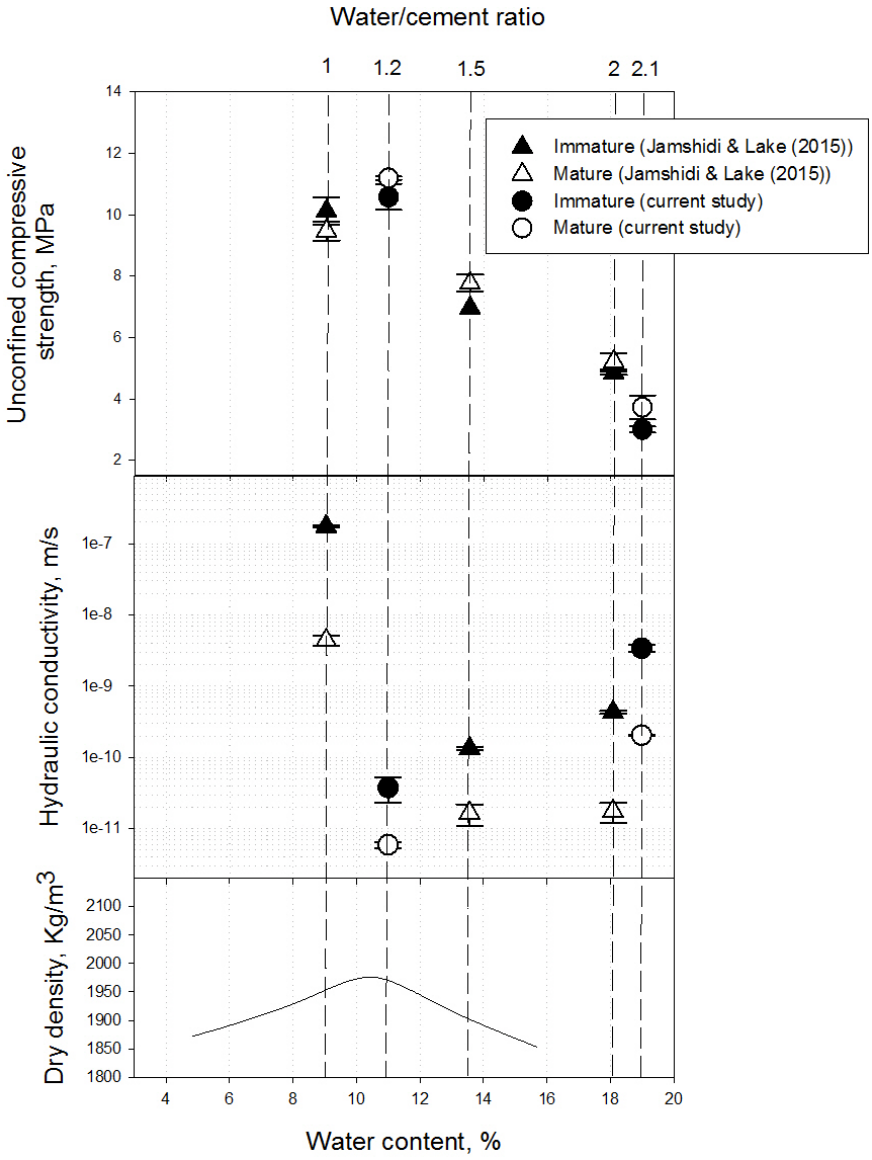

Figure 3: Variations of the hydraulic conductivity and UCS with respect to the changes in the water content in the mix design (control samples).

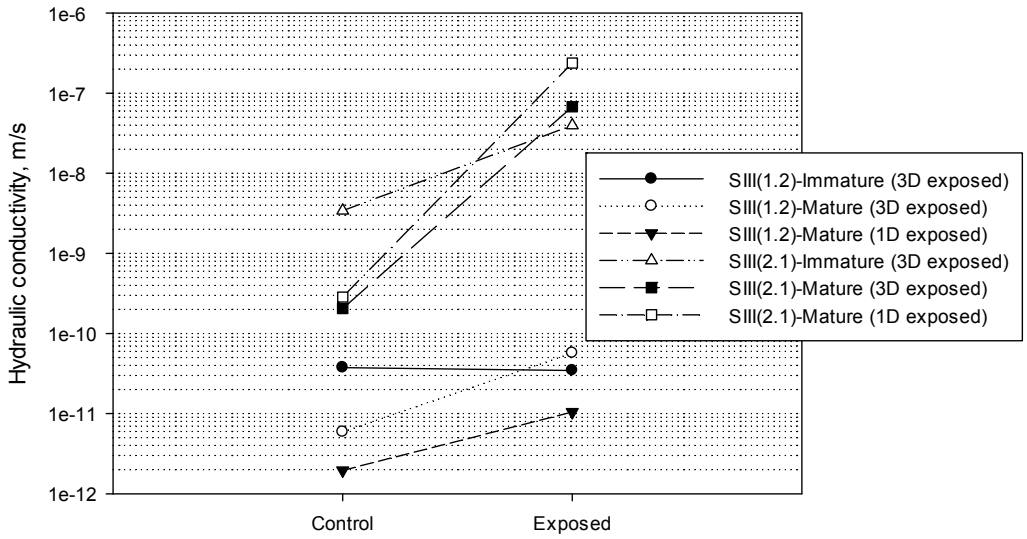

Figure 4: Changes in the hydraulic conductivity of specimens after three cycles of f/t exposure. See Table 3 for the relative standard deviation values within measurements.

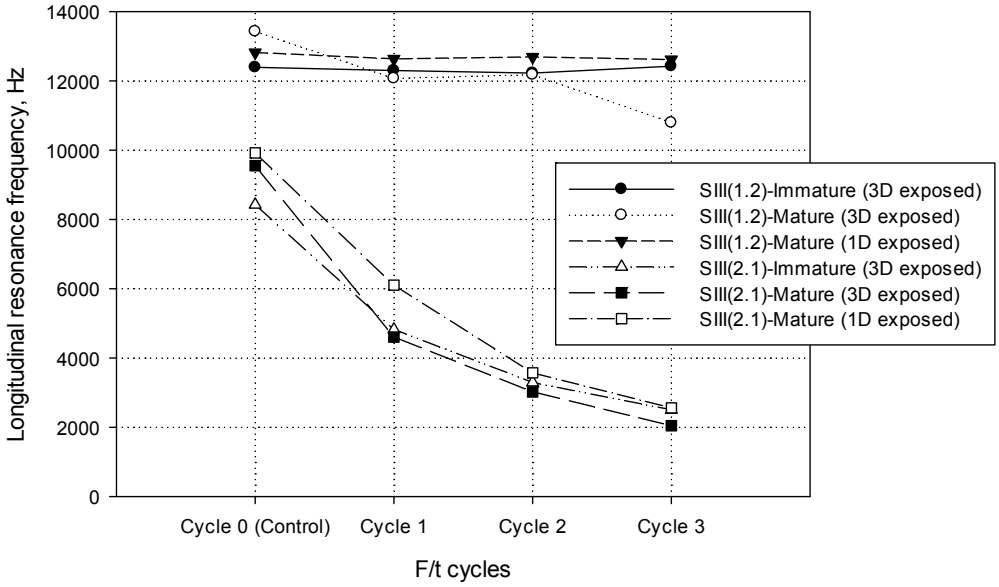

Figure 5: Variation of RF values at different f/t cycles. See Table 3 for the relative standard deviation values within measurements.

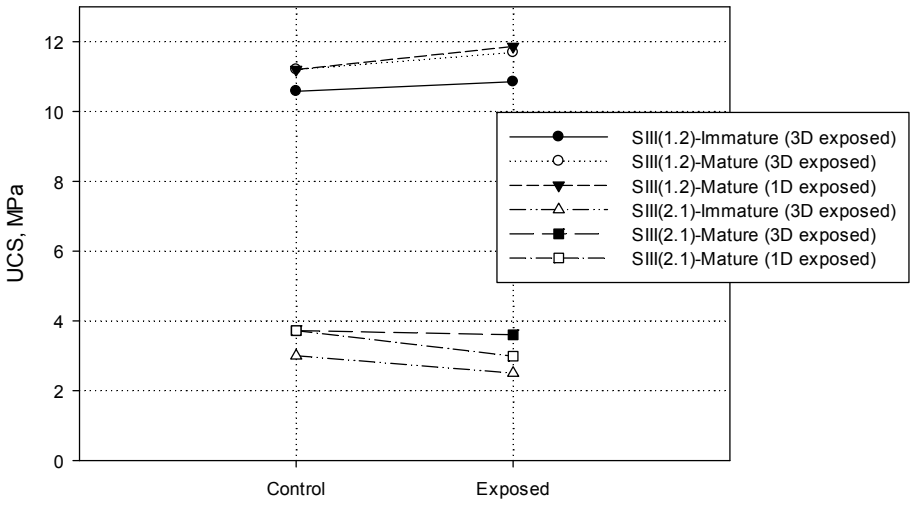

Figure 6: Comparison of UCS values for control (i.e. unexposed) and exposed conditions. See Table 3 for the relative standard deviation values within measurements.

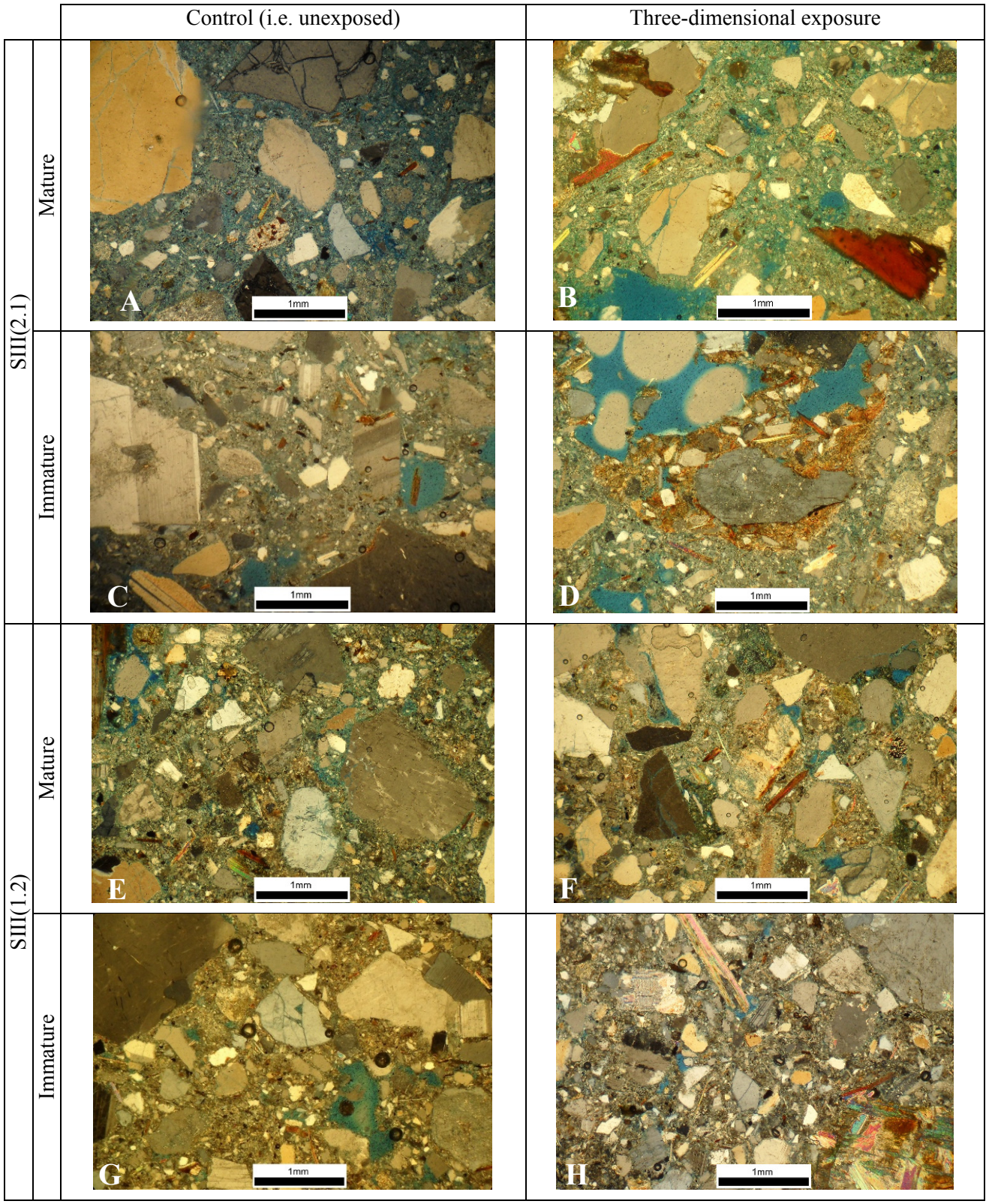

Figure 7: Typical micrographs from vertical planes of specimens under various curing and exposure scenarios.

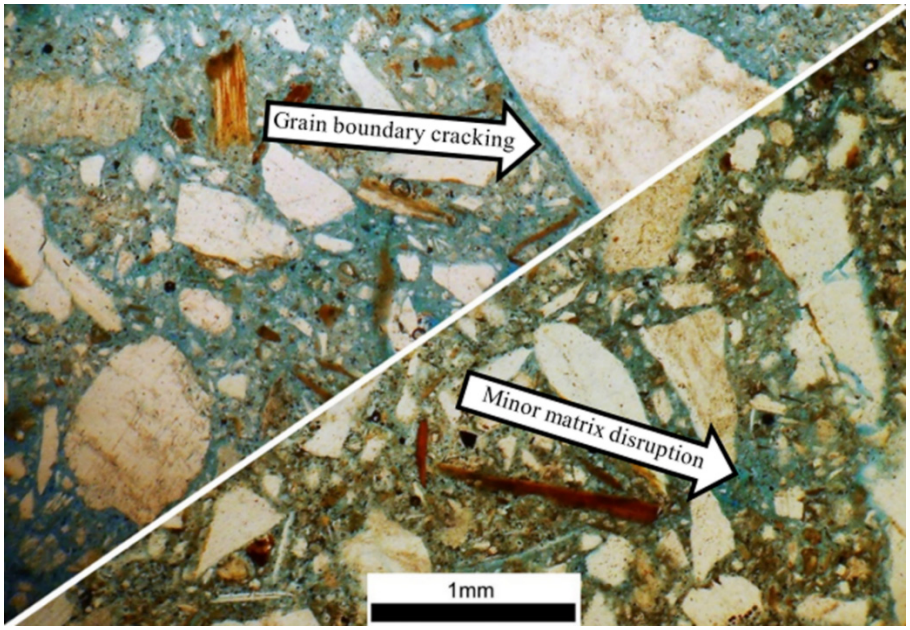

Figure 8: Micrographs taken from SIII(2.1)-immature ($K_{exposed}/K_0 \approx 12$) specimens (bottom corner) and SIII(2.1)-mature ($K_{exposed}/K_0 \approx 320$) specimens (top corner) under three-dimensional f/t exposed conditions.

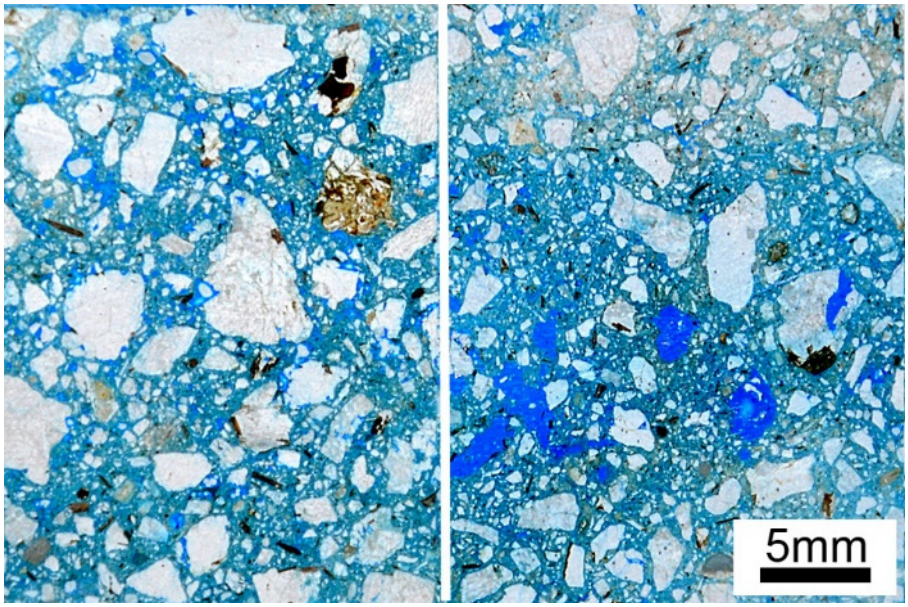

Figure 9: Damage formation in SIII(2.1)-mature at macro scale. Left: control; right: three-dimensional exposed conditions.

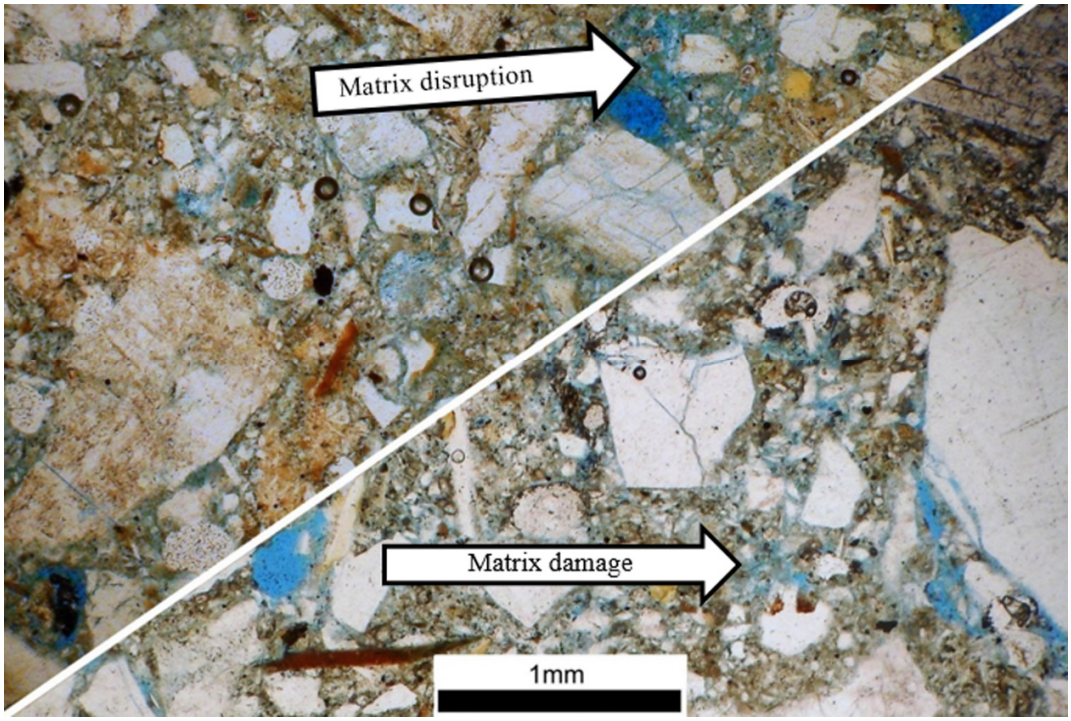

Figure 10: Micrographs taken from SIII(1.2)-immature specimens (bottom right) and SIII(1.2)-mature specimens (top left) under three-dimensional f/t exposed conditions.

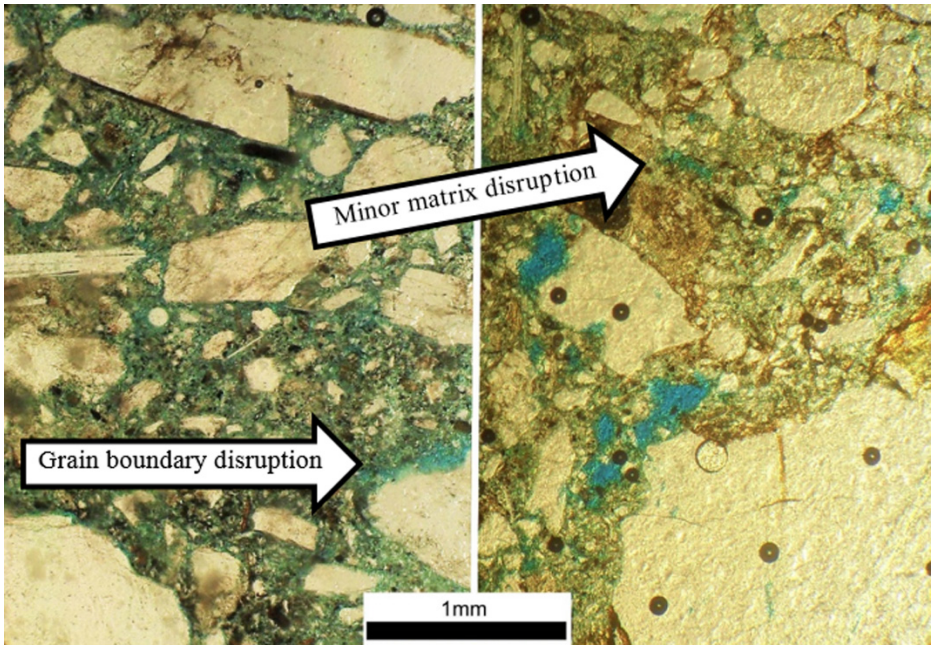

Figure 11: Micrographs taken from SIII(2.1)-mature specimens (left) and SIII(1.2)-mature specimens (right) under one-dimensional f/t exposed conditions.